Eleventh International Conference on Computational Fluid Dynamics (ICCFD11), Maui,Hawaii, July 11-15, 2022

ICCFD11-2022-1202

A Zonal Direct-Hybrid Aeroacoustic Simulation Framework Using a High-Order Discontinuous Galerkin Spectral Element Method

D. Kempf*and C.-D. Munz*
Corresponding author: daniel.kempf@iag.uni-stuttgart.de

*Institute of Aerodynamics and Gas Dynamics, University of Stuttgart, Germany

Abstract: This work presents a zonal direct-hybrid aeroacoustic simulation framework using a high-order discontinuous Galerkin spectral element method. We combine a zonal large eddy simulation (LES) approach with an acoustic propagation solver in a direct-hybrid manner. In the zonal approach, we use the recycling rescaling anisotropic linear forcing method as turbulent inflow at the interface of the Reynolds-averaged Navier-Stokes equations (RANS) and the LES. This method relies upon provided turbulent statistics to generate turbulence. Based on a RANS simulation, we use the recently proposed simple and robust method to model the required Reynolds stresses using the distribution of the turbulent kinetic energy obtained from the turbulence model. For the computational aeroacoustic simulation, we follow a direct-hybrid simulation approach by simultaneously performing the zonal LES and acoustic propagation simulation. The acoustic sources are directly exchanged between the two solvers, omitting frequent slow I/O operations. Due to the synchronization of both simulations, to achieve the optimal performance, we use a static load balancing. To validate the framework, we present simulation results of a zonal direct-hybrid trailing edge simulation of a NACA 64418 airfoil at $Re = 10^6$.

Keywords: Hybrid RANS-LES Method, Computational Aeroacoustics, High-Order Method.

1 Introduction

In computational aeroacoustics (CAA), hybrid simulation approaches are state of the art [1]. The advantage of the classical hybrid simulation approach is that the flow field and the acoustic propagation are simulated independently. In doing so, the challenging multi-scale character of aeroacoustics is tackled by a separation of the scales of hydrodynamics and acoustics.

The quality of CAA methods depend, among other things, on the accurate prediction of the hydrodynamics and the extracted acoustic sources. In industrial applications with a focus on high computational efficiency, low-fidelity methods, like solving the (unsteady) Reynolds-averaged Navier-Stokes equations (RANS), are frequently used to predict the flow field, often in combination with statistical modeling of the acoustic sources. Besides their computational efficiency, the downside is that models can be inaccurate in complex flow regimes like separation. With increased computing power, high-fidelity methods, such as wall resolved large eddy simulations (LES), become more and more relevant for industrial applications. However, wall resolved LES of large configurations are yet not computationally feasible. Zonal RANS-LES approaches are used more often e.g. by König et al. [2], Erbig and Maihöfer [3] and Kuhn et al. [4] and are also used in the CAA community. Bernicke et al. [5] and Satcunanathan et al. [6] use a zonal LES approach to predict the noise of porous trailing edges of airfoils. Bernicke et al. extract acoustic source terms in the zonal region and perform a 2D CAA simulation for far-field noise.

Traditionally, in hybrid CAA of low Mach number cases, the acoustic sources are extracted from an incompressible flow simulation. In this case, certain aeroacoustic effects like acoustic feedback cannot be predicted due to a neglected interaction of hydrodynamics and acoustics. However, acoustic feedback can be relevant in developing technical products. By solving the compressible Navier-Stokes equations (NSE) these effects can be captured in direct noise computation (DNC). Using DNC, Frank and Munz [7] predicted aeroacoustic feedback on a side-view mirror, Kuhn et al. [4] and Ergib and Maihöfer [3] predicted Rossiter feedback on cavity configurations relevant to the automotive industry. Therefore, there are cases in which, even at low Mach number, solving the compressible NSE is beneficial.

In this work, we present the extension of the discontinuous Galerkin framework FLEXI[1] towards zonal hybrid CAA. We solve the flow field and the acoustic propagation with the same underlying discontinuous Galerkin scheme. In the zonal LES approach, we solve the compressible NSE and we use the recycling rescaling anisotropic linear forcing (RRALF) introduced by Kuhn et al. [8] to generate the inflow turbulence. This turbulent inflow method requires the time-averaged mean velocities and the full Reynolds stress tensor as input data. We use a modeling approach to model the full Reynolds stress tensor based on 2D or 3D RANS simulations described in Kempf and Munz [9]. The acoustic propagation is done by solving the acoustic perturbation equations (APE) in version 4 by Ewert and Schröder [10]. We perform the flow and acoustic propagation simulations simultaneously and interchange the acoustic sources directly. To account for the different computational efforts between the two solvers and the synchronization within each timestep, we apply a static load balancing to achieve optimal performance.

First, we present the numerical framework we use to perform zonal direct-hybrid acoustic simulations. Following, we present the results of a zonal direct-hybrid acoustic simulation of a NACA 64418 trailing edge at $Re = 10^6$.

2 Numeric Method

High-order methods are beneficial when dealing with turbulence and acoustics due to their low dissipation and dispersion errors [11]. In this work, we use the discontinuous Galerkin method implemented in our framework FLEXI [12]. This framework has been successfully applied to DNC simulations [7, 4]. The extension towards a zonal hybrid framework is described in the following and follows Kempf and Munz [9, 13]. We further discuss the performance impact of the static load-balancing of the direct-hybrid framework.

2.1 Discontinuous Galerkin Spectral Element Method

This work considers the compressible NSE, which intrinsically include the hydrodynamics and acoustics, and the APE-4 equation system proposed by Ewert and Schröder [10] used for the acoustic propagation. We solve both systems of equations with the discontinuous Galerkin spectral element method (DGSEM).

To numerically solve the system of equations with the DGSEM, we discretize the physical domain with three-dimensional, non-overlapping hexahedral elements. For a better representation of the geometry, we use curved elements, and for flexible meshing we allow an unstructured mesh topology. Each element is transformed from the physical space to the unit reference element $E = [-1;1]^3$, where $\vec{\xi} = [\xi^1, \xi^2, \xi^3]$ represents the reference coordinates. The transformation follows Kopriva [14]. We obtain the variational form by multiplying a basis function by a test function ϕ, which is chosen in the Galerkin approach identical to the basis function. As basis functions, we choose a tensor product of one-dimensional Lagrange polynomials. Integrating over the reference element E and integration by parts yields the weak formulation of the DGSEM

$$\frac{\partial}{\partial t}\int_E JU\phi \, d\vec{\xi} + \oint_{\partial E} (\mathcal{G}_n^* - \mathcal{H}_n^*)\phi \, ds - \int_E \vec{\mathcal{F}} \cdot \vec{\nabla}_\xi \phi \, d\vec{\xi} = 0, \tag{1}$$

where $\mathcal{G}^*$ and $\mathcal{H}^*$ denoted numerical flux function normal to the surface for the inviscid and the viscous term, respectively. In the case of the NSE the volume flux is $\mathcal{F} = \mathcal{F}(U, \vec{\nabla}_x U)$, and in the inviscid APE-4 case, the viscous flux $\mathcal{H}^*$ vanishes, and the volume flux is $\mathcal{F} = \mathcal{F}(U)$.

We use the Legendre-Gauss-Lobatto quadrature for integration and interpolation points, yielding a collocation approach following Kopriva [15]. We use the Roe and the Lax–Friedrichs Riemann flux [16] to determine the inviscid surface flux at the cell interface in the case of the NSE and the APE-4 equation system. To approximate the viscous flux of the NSE system, we use the lifting procedure of Bassi and Rebay [17]. To stabilize the DGSEM, we use the kinetic energy preserving split flux form proposed by Gassner et

[1] www.flexi-project.org

al. [18] and implemented by Flad et al. [19]. As the time integration scheme, we apply the low storage fourth order explicit Runge-Kutta method of Carpenter and Kennedy [20].

The treatment of the boundaries is crucial when dealing with acoustics. To prevent artificial reflections of acoustic waves and the turbulent flow structures we use a sponge zone proposed by Pruett [21] and boundary conditions of Dirichlet type in weak form. Further details about the implementation and the acoustic properties of the DGSEM can be found in Flad et al. [22].

2.2 Target Data Generation

For the the ALF and the static rescaling, we need to provide target data, namely the time-averaged mean velocities and the Reynolds stress distribution in the turbulent inflow region. We use data provided by a simulation solving the RANS equations using Menter's shear stress transport turbulence model. We obtain the time-averaged mean velocities directly from the simulation. The distribution of the Reynolds stresses is not modeled in the turbulence model, only the turbulent kinetic energy k and the turbulent dissipation rate ω. There is the possibility of using a Reynolds stress transport model, but these are not very commonly used. In this work, we use a simple model approach to approximate the full Reynolds stress tensor based on the scaling of the distribution of k. The approach is based on the findings of Bradshaw et al. [25]. In this one equation turbulence model, the shear stress $\overline{u_1'u_2'}$ is modeled by a constant scalar scaling of the turbulent kinetic energy k. In this work, we use the extension to the full Reynolds stress tensor by Kempf and Munz [9]. Therefore, instead of a single scalar, we define a symmetric tensor S_{ij} with an individual scaling scalar for each Reynolds stress tensor component. Here, the trace of tensor S_{ij} must be exactly two to conserve the turbulent kinetic energy k. To generalize the model, the sign of the Reynolds stresses approximated by Boussinesq's assumption specifies the appropriate sign of the Reynolds stresses. The model is described in Eq. 2. In Fig. 1 the Reynolds stresses normalized by the turbulent kinetic energy k of a wall resolved LES are plotted for the case of a NACA 64418 airfoil. Fig. 1 indicates that the assumption of a constant scaling factor is valid for the outer region of the boundary layer. These factors are also only slightly varying for different attached flow configurations.

$$\overline{u_i'u_j'} = \mathrm{sgn}\left(-\nu_t\left(\frac{\partial u_i}{\partial x_j}+\frac{\partial u_j}{\partial x_i}\right)+\frac{2}{3}\delta_{ij}k\right)S_{ij}k \tag{2}$$

Fig. 2 displays the modeled Reynolds stresses of the NACA 64418 airfoil compared to a wall resolved LES at the same position. We follow the strategy of skipping the region near the wall when applying the ALF. Therefore, we skip the region with the largest modeling errors and rely on the natural development of the turbulence in the near-wall region. This approach is valid due to the recycling and rescaling part of the RRALF method, which allows for the rapid natural development of the near-wall turbulence.

2.3 Computational Aeroacoustic Simulation Framework

Within the scope of this work, we use the extension of the framework FLEXI towards a framework capable of performing hybrid acoustic simulations. Besides solving the compressible NSE, we also solve the APE-4 equation system proposed by Ewert and Schröder [10]. We use the perturbed Lamb vector $L' = [\omega \times u]'$ as an acoustic source at low Mach number cases. In the region where acoustic production is assumed e.g., at the trailing edge of an airfoil, the Lamb vector is extracted from a zonal LES, solving the compressible NSE.

There are two possibilities to perform the hybrid acoustic simulation implemented within this framework. First, the simulation to determine the acoustic sources is carried out independently, and the acoustic sources are extracted and stored. Here, the acoustic sources do not have to be stored at every explicit time step to achieve good quality results. The applied acoustic sources are then interpolated to the required time step in the acoustic propagation simulation. Such a hybrid simulation requires a lot of storage space and complicates the handling of hybrid acoustic simulations.

The second approach is to compute the flow and the acoustic propagation simulation simultaneously. This offers the advantage of directly communicating the extracted acoustic sources to the acoustic solver. This approach omits to save the acoustic sources. The resulting reduction of required I/O operations makes this approach well suited for large-scale simulations done in high-performance computing. Further, an exchange of the acoustic sources at each time step or even at each Runge-Kutta stage is possible without significant

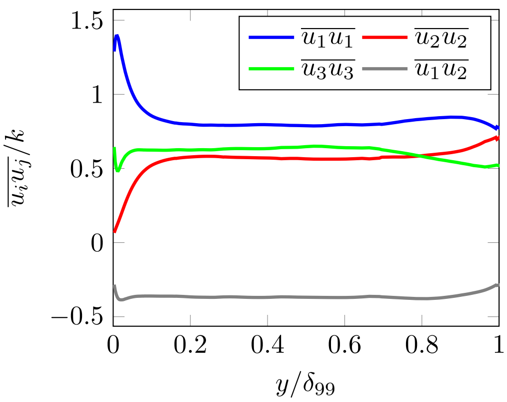

Figure 1: Reynolds stresses normalized by the turbulent kinetic energy k. Plotted in wall-normal direction on the suction side of a NACA 64418 airfoil.

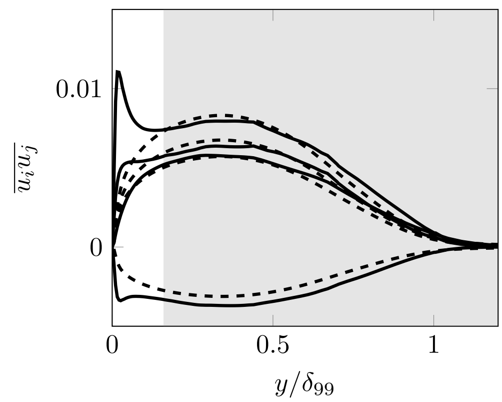

Figure 2: Comparison of modeled Reynolds stresses (dashed) and results of a wall resolved LES (solid). Plotted in wall-normal direction on the suction side of a NACA 64418 airfoil. The values used for the scaling tensor S_{ij} are $S_{11} = 0.8$, $S_{22} = 0.55$, $S_{33} = 0.65$ and $S_{12} = 0.3$. The area where the ALF is applied is indicated in gray.

impact on the performance compared to the approach of storing the acoustic sources. This also prevents the uncertainty of a negative impact due to the temporal resolution of the source data. Within each timestep, we synchronize the minimal timestep of both solvers. Thereby, and due to the larger computational effort to solve the NSE, a static load balancing is introduced between both solvers. Solving the NSE is approximately twice as expensive as solving the APE-4 equation system within this DG framework. First, as a baseline, we measured the baseline performance of each individual solver by computing a sample case of $64 \times 64 \times 32$ elements and a polynomial degree of $N = 5$ with a varying number of CPU cores from 2,048 to 16,384. The different performance at varying load is plotted in Fig. 3a for the non-synchronized execution of the flow solver (NS) and the acoustic propagation solver (APE-4). Here, we use the performance index (PID) as a metric for the performance, which is defined as

$$\mathrm{PID} = \frac{\text{wall-clock-time} \cdot \#\text{cores}}{\#\text{DOF} \cdot \#\text{time steps} \cdot \#\text{RK-stages}} \ , \tag{3}$$

and describes the time it takes a core on average to update a single degree of freedom (DOF) for one Runge-Kutta stage. The performance of DGSEM framework is usually bounded by the available memory bandwidth. This results in a noticeable loss in performance towards higher loads. At loads below the here presented values, we typically see again a loss in performance due to decreased local work resulting in a higher sensitivity to the latency of the communication. For a more in-depth discussion of the performance properties of our framework, the interested reader is referred to Krais et al. [12] and Kempf et al. [26]. Fig. 3a indicates that the acoustic propagation solver offers a larger range of different loads with optimal performance. Whereas the flow solver shows a smaller window of optimal performance. Therefore, our objective for the static load balancing is to perform the simulation of the flow solver at its optimal performance and use the favorable properties of the acoustic propagation solver and optimize the load for overall performance.

In Fig. 3b the performance of each individual solver is plotted for the synchronized case. Here, the load of the flow solver is fixed at the value indicated in Fig. 3a by the vertical line and the load of the acoustic propagation solver is varied. The minimal timestep of both solvers is synchronized at each timestep. The exchange interval of the acoustic source data is plotted for $n_{ex} = 1, 10$ and 100, meaning for $n_{ex} = 10$ the acoustic sources are exchanged each 10^{th} timestep. In case $n_{ex} > 1$ the acoustic solver buffers the source data of four time instances and performs a third-order interpolation in time. As displayed in Fig. 3b, towards low loads the impact of the synchronization of the timestep gets dominant. Here, during the synchronization

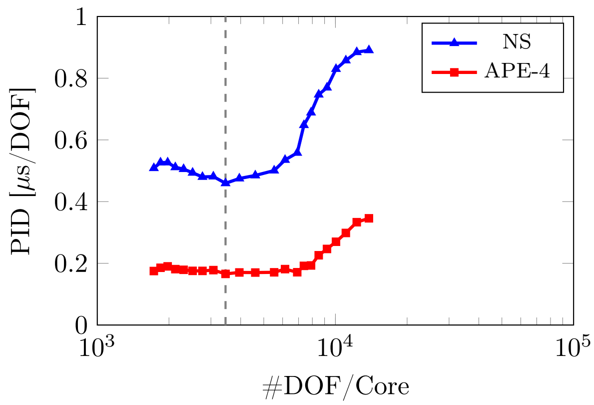

(a) The baseline performance of the unsynchronized flow solver (NS) and acoustic propagation solver (APE-4) at different loads.

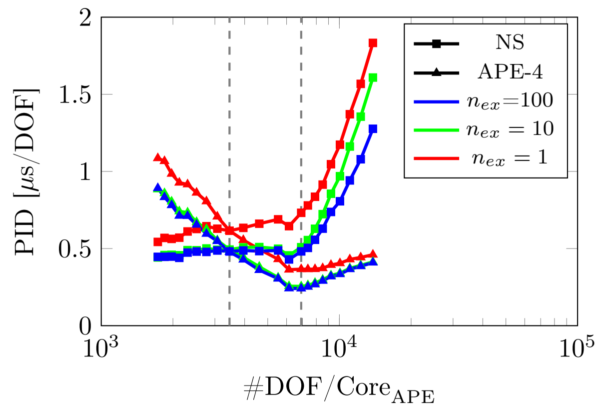

(b) Performance of the synchronized simulation. Flow solver at optimal performance and a varying load of the acoustic solver at different source exchange rates n_{ex}.

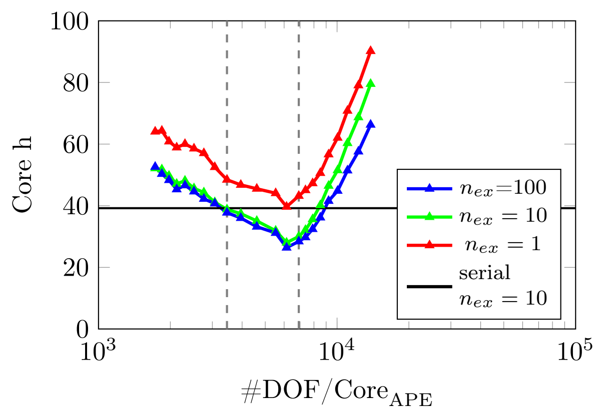

(c) Wall time of the combined solvers. Wall time of serial execution of both solvers and storing of the acoustic sources at $n_{ex} = 10$, both solvers using an optimal load.

Figure 3: Performance analysis of the direct-hybrid approach. Comparison of the synchronized solvers to the stand-alone execution and investigation of the impact of the acoustic source exchange rate N_{ex}.

the flow solver has a significant idling time. Towards high loads the computation and communication of the source data get the restricting factor. Despite implementing all communications between the two solvers in a non-blocking manner allowing for a staggered execution, we observe at frequent exchange rates between $n_{ex} = 1$ and $n_{ex} = 10$ an impact performance that vanishes for higher exchange rates in the relevant ranges of load. In the direct hybrid case, we achieve an optimal performance of the acoustic propagation solver using an about 1.7 times higher load in the acoustic propagation simulation with a slight loss of performance in the flow solver. In Fig. 3c the overall performance in terms of effective combined wall time is plotted. Here, we observe the same behavior regarding the exchange rate of the acoustic sources. Again, we see the best overall performance using an about 1.7 times higher load in the acoustic propagation simulation. The horizontal line plotted in Fig. 3c indicates the required wall time, including I/O, of the traditional approach of storing and reading the acoustic sources. At the example of writing and reading the source data at each 10^{th} timestep leads to an overhead of about 40% compared to the optimal direct-hybrid case. This obviously strongly depends on the available hardware and I/O performance. Generally speaking, a more frequent exchange of the acoustic source data favors the second approach whereas less frequent favors the first approach. We also want to highlight that the first approach can profit from reusing the stored acoustic sources resulting in a potentially overall more efficient approach. We see the advantage of the direct-hybrid approach in high-performance computing. This approach is beneficial in the case of large-scale simulations with only a few executions. Here, we do not greatly profit from the possible reusability of the acoustic source data by storing them. Also, large-scale simulations likely produce a huge amount of data to be handled and stored.

Further, to capture the convection and refraction in the acoustic simulation and to compute the perturbed Lamb vector, we need to provide mean flow data. This can be done by time-averaging a precursor simulation or, in the case of hybrid simulations without precursor simulation, e.g., in the direct-hybrid case, by computing a moving average in the flow solver and communicating it to the acoustic solver. Within this work, we use the same mesh for both solvers, and we chose the second approach.

3 Simulation Results

We applied the described framework to the zonal direct-hybrid acoustic simulation of a NACA 64418 airfoil's trailing edge. Here, we validate the results of the flow field based on the model described in Sec. 2.2 against results based on target data obtained from a wall resolved LES of the airfoil. The results of the acoustic propagation are validated against the zonal DNC. The following results follow Kempf and Munz [13], and a more in-depth analysis of the hybrid acoustic framework can be found in Kempf and Munz [9].

3.1 Zonal Hybrid Acoustic Simulation: NACA 64418 Airfoil

We carried out a hybrid acoustic simulation based on a zonal LES of a NACA 64418 airfoil. The airfoil has an angle of attack of 6 degrees, a free-stream Mach number of $Ma = 0.2$, and a Reynolds number of $Re = 10^6$. The setup is displayed in Fig. 4. The simulation setup contains the trailing edge of the airfoil. In the background, the mesh, consisting of 58,800 high-order cells, is displayed. The recycling planes on the suction and pressure side and the inflow planes are displayed. Between the recycling and the inflow planes, the region where the forcing is active is displayed in blue. Behind the recycling plane, the turbulent vortex structures are visualized by the Q-criterion $Q = 200$ and colored by the streamwise velocity component.

In a first step, we simulated a zonal LES of the trailing edge with target data derived by the method described in Sec. 2.2 and validated it against a wall resolved LES of the whole airfoil. The mean velocity field showsover all a very good agreement with the reference. In Fig. 5 we present the distribution of the velocity fluctuations at the inflow, behind the ALF region and at the trailing edge, on the suction side and pressure side, and at three positions in the wake. The zonal simulation shows very good agreement with the full LES in the mean velocity field. Directly at the inflow plane, the deviations from the reference are the largest. Due to the recycling of the fluctuations to the inflow and the pressure gradient on the suction and pressure side, the shape of the distribution of the velocity fluctuations differs from the reference. In the following, the distribution trends towards the reference. This is due to the correction by the ALF and the natural development of the turbulence. The good agreement of the distributions at the trailing edge results

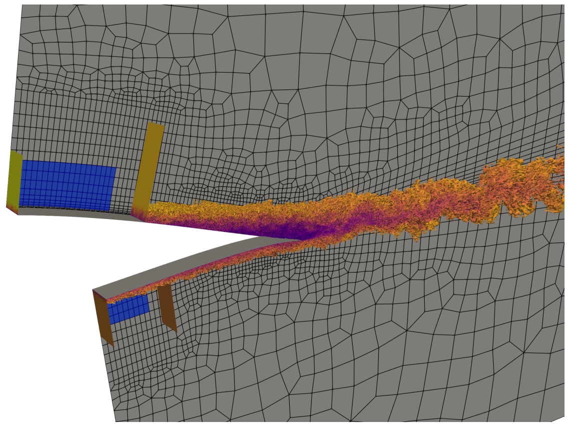

Figure 4: Trailing edge of the NACA 64418 airfoil. Vortex structure visualized by the Q-criterion (Q=200) colored by the streamwise velocity in the range [-0.3, 1.3]. Displayed planes indicate the inflow and recycling planes on the suction and pressure side. The forcing region is displayed in blue.

in also a good agreement in the wake. This agreement is quite important since the region at the trailing edge has a huge impact on the generation of acoustic emissions.

In Fig. 6 the acoustic power spectrum of the acoustic propagation simulation and the DNC of the zonal LES are plotted. The spectrum is evaluated 0.2 chord length above the trailing edge. In the high frequencies, we see a good agreement with the reference DNC. The decline and the amplitude of the acoustic level are comparable, both for the zonal DNC and for the acoustic propagation simulation. At low frequencies, the zonal DNC has a higher noise level. This is the influence of the turbulent inflow method, which generates artificial noise. We extract the acoustic sources only after the turbulent inflow region. Therefore we reduce the amount of artificial noise in the acoustic propagation simulation. This is also our motivation to use this kind of hybrid approach.

4 Conclusion

We presented simulation results of a new method for direct-hybrid zonal aeroacoustic analyses implemented in the high-order discontinuous Galerkin framework FLEXI. High-order schemes, such as discontinuous Galerkin, are well suited for acoustic simulations due to their beneficial dissipation and dispersion properties. To simulate the flow field, we solve the compressible Navier-Stokes equations (NSE) within this framework with a high-order discontinuous-Galerkin scheme. We recently extended the framework with an acoustic propagation solver, where we solve the acoustic perturbation equations in version 4 with the same high-order discontinuous Galerkin scheme. We use the perturbed Lamb vector in vortex noise-dominated problems as an acoustic source. Solving the compressible NSE equations already allows the prediction of the acoustic field and also depicts acoustic flow interaction. However, due to the high computational cost of direct noise computation (DNC), our approach is to restrict the highly resolved flow field to the relevant acoustic source region using zonal large eddy simulation (LES). We extract the Lamb vector from the zonal LES and use it as an acoustic source in the acoustic propagation simulation.

The zonal LES approach requires a turbulent inflow method. We use the recycling rescaling anisotropic linear forcing, a combination of the traditional recycling rescaling approach with an anisotropic linear forcing. This method produces turbulence at the inflow with high-quality as needed to predict the acoustic sources. It requires a time-averaged mean velocity field and the full Reynolds stress tensor as input values. We perform a RANS simulation to predict the mean velocity field and the distribution of the turbulent kinetic energy. Based on the distribution of the turbulent kinetic energy, we model the distribution of the Reynolds stresses

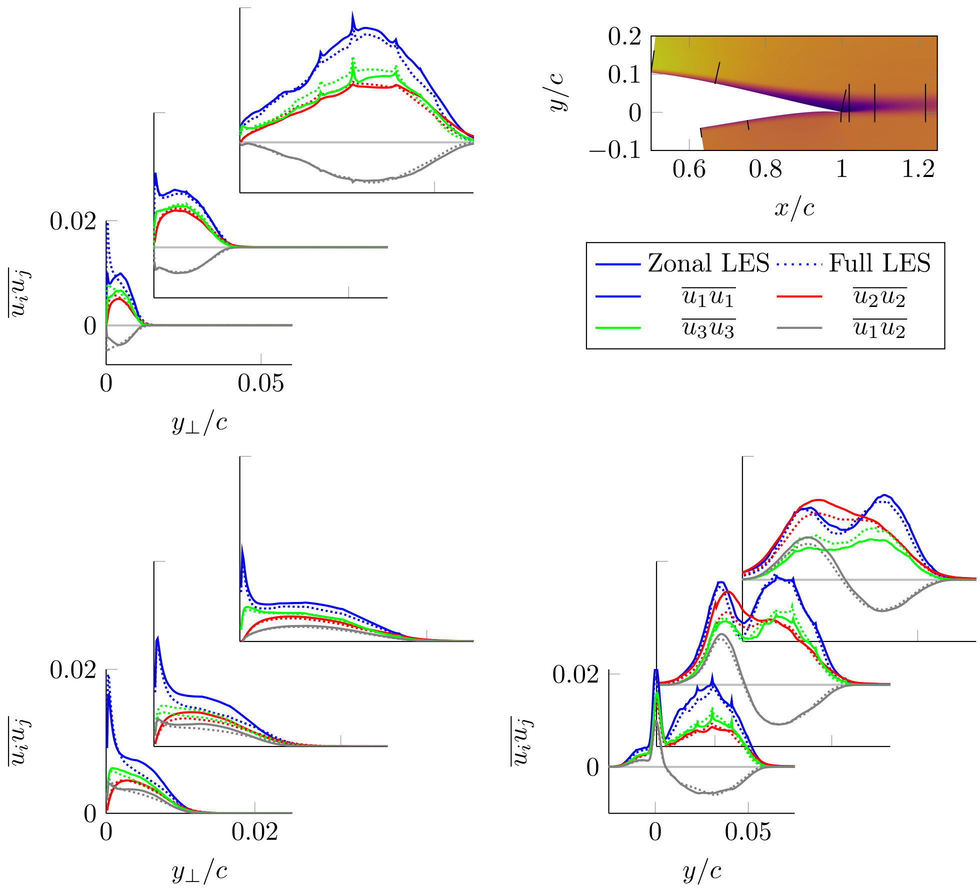

Figure 5: Velocity fluctuation profiles in comparison to the full LES at the displayed positions. Profiles stagered in streamwise direction. Top left: suction side. Top right: mean streamwise velocity including the possitions of the velocity fluctuation profiles. Bottom left: pressure side. Bottom rigth: wake region.

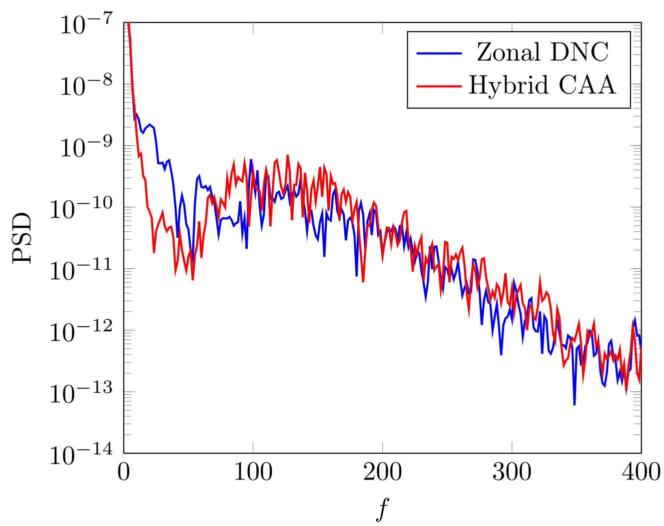

Figure 6: PSD of the dimensionless pressure 0.2 chord length above the trailing edge. Comparison of the hybrid CAA simulation and the zonal DNC.

by anisotropic scalar scaling.

We perform the hybrid simulation in a direct manner, meaning we simultaneously perform the flow and acoustic solver and exchange the acoustic sources directly between the solver. Du to the different computational efficiency of both solvers and a synchronization of the minimal timestep, we use a static load balancing between both solvers. We presented performance analyses demonstrating the benefits of using the static load balancing. Further, we showed that a very frequent exchange rate of the acoustic sources does not strongly impact the performance. Also, we presented an example of 40% performance gain compared to the classical approach of storing the acoustic source data.

Using the example of a NACA 64418 airfoil's trailing edge, we applied both building blocks of the zonal hybrid acoustic simulation, the turbulent inflow based on RANS simulation data and the acoustic propagation solver. The presented zonal framework is capable of reproducing the Reynolds stress distribution very well compared to a reference simulation, especially in the relevant region at the trailing edge and in the wake. This proves the approach used to model the Reynolds stress distribution in combination with the turbulent inflow method to be well suited. We compare the acoustic emissions between the acoustic propagation solver and the DNC results of the zonal LES. At high frequencies, the results show similar behavior. At low frequencies, the acoustic results of the zonal LES show the influence of the turbulent inflow. Here, artificial noise is produced, and a higher noise level is predicted. In the acoustic propagation solver, we omit the acoustic sources in the inflow region. This strongly reduces the amount of artificial noise in the acoustic simulation.

The results of the zonal hybrid simulation approach show great potential. Computing the acoustic sources in a zonal manner opens the possibility of using high-fidelity methods to compute the acoustic sources efficiently. In combination with an acoustic propagation solver, the prediction of far-field noise beyond the restricted LES domain is feasible.

Acknowledgments

The authors gratefully acknowledge the support and computing resources granted by the High Performance Computing Center Stuttgart (HLRS) on the national supercomputer HPE Apollo (Hawk) under the grant hpcdg. Also we want to acknowledge the support of the Deutsche Forschungsgemeinschaft (DFG, German Research Foundation) under Germany's Excellence Strategy - EXC 2075 - 390740016.

References

[1] M Kaltenbacher, M Escobar, S Becker, and I Ali. Numerical simulation of flow-induced noise using les/sas and lighthill's acoustic analogy. *International journal for numerical methods in fluids*, 63(9):1103–1122, 2010.

[2] Daniel König, Matthias Meinke, and Wolfgang Schröder. Embedded les-to-rans boundary in zonal simulations. *Journal of Turbulence*, (11):N7, 2010.

[3] Lars Erbig and Martin Maihöfer. A hybrid rans/les for automotive gap noise simulations. In *25th AIAA/CEAS aeroacoustics conference*, page 2445, 2019.

[4] Thomas Kuhn. Zonal large eddy simulation of active open cavity noise using a high order discontinuous galerkin method. In *25th AIAA/CEAS aeroacoustics conference*, page 2465, 2019.

[5] Paul Bernicke, RAD Akkermans, Varun B Ananthan, Roland Ewert, Jürgen Dierke, and Lennart Rossian. A zonal noise prediction method for trailing-edge noise with a porous model. *International Journal of Heat and Fluid Flow*, 80:108469, 2019.

[6] Sutharsan Satcunanathan, Matthias Meinke, and Wolfgang Schroeder. Numerical analysis of poro-serrated trailing-edge noise. In *28th AIAA/CEAS Aeroacoustics 2022 Conference*, page 2817, 2022.

[7] Hannes M Frank and Claus-Dieter Munz. Direct aeroacoustic simulation of acoustic feedback phenomena on a side-view mirror. *Journal of sound and vibration*, 371:132–149, 2016.

[8] Thomas Kuhn, Daniel Kempf, Andrea Beck, and Claus-Dieter Munz. A novel turbulent inflow method for zonal large eddy simulations with a discontinuous Galerkin solver. *Submitted for publication in Computers and Fluids*, 2020.

[9] Daniel Kempf and Claus-Dieter Munz. Zonal direct-hybrid aeroacoustic simulation of trailing edge noise using a high-order discontinuous galerkin spectral element method. *Submitted for publication in Acta Acustica*, 2022.

[10] Roland Ewert and Wolfgang Schröder. Acoustic perturbation equations based on flow decomposition via source filtering. *Journal of Computational Physics*, 188(2):365–398, 2003.

[11] Gregor Gassner and David A Kopriva. A comparison of the dispersion and dissipation errors of gauss and gauss–lobatto discontinuous galerkin spectral element methods. *SIAM Journal on Scientific Computing*, 33(5):2560–2579, 2011.

[12] Nico Krais, Andrea Beck, Thomas Bolemann, Hannes Frank, David Flad, Gregor Gassner, Florian Hindenlang, Malte Hoffmann, Thomas Kuhn, Matthias Sonntag, and Claus-Dieter Munz. Flexi: A high order discontinuous Galerkin framework for hyperbolic–parabolic conservation laws. *Computers and Mathematics with Applications*, 2020.

[13] Daniel Kempf and Claus-Dieter Munz. Zonal hybrid computational aeroacoustics simulation of trailing edge noise using a high-order discontinuous galerkin method. In *28th AIAA/CEAS Aeroacoustics 2022 Conference*, page 3021, 2022.

[14] David A. Kopriva. Metric identities and the discontinuous spectral element method on curvilinear meshes. *Journal of Scientific Computing*, 26(3):301, 2006.

[15] David A. Kopriva. *Implementing spectral methods for partial differential equations: Algorithms for scientists and engineers.* Springer Science & Business Media, 2009.

[16] Eleuterio F. Toro. *Riemann solvers and numerical methods for fluid dynamics: a practical introduction.* Springer Science & Business Media, 2013.

[17] Francesco Bassi and Stefano Rebay. A high-order accurate discontinuous finite element method for the numerical solution of the compressible navier–stokes equations. *Journal of computational physics*, 131(2):267–279, 1997.

[18] Gregor J Gassner, Andrew R Winters, and David A Kopriva. Split form nodal discontinuous galerkin schemes with summation-by-parts property for the compressible euler equations. *Journal of Computational Physics*, 327:39–66, 2016.

[19] David Flad and Gregor Gassner. On the use of kinetic energy preserving dg-schemes for large eddy simulation. *Journal of Computational Physics*, 350:782–795, 2017.

[20] Mark H. Carpenter and Christopher A. Kennedy. *Fourth-order 2N-storage Runge-Kutta schemes.* Technical Report, NASA-TM-109112, 1994.

[21] Dave Pruett, Thomas Gatski, Chester Grosch, and William Thacker. The temporally filtered Navier-Stokes equations: properties of the residual stress. *Physics of Fluids*, 15(8):2127–2140, 2003.

[22] David Flad, Hannes Frank, Andrea Beck, and Claus-Dieter Munz. A discontinuous Galerkin spectral element method for the direct numerical simulation of aeroacoustics. *AIAA Paper (2014-2740)*, 2014.

[23] B De Laage de Meux, B Audebert, Remi Manceau, and R Perrin. Anisotropic linear forcing for synthetic turbulence generation in large eddy simulation and hybrid RANS/LES modeling. *Physics of Fluids*, 27(3):035115, 2015.

[24] Thomas S Lund, Xiaohua Wu, and Kyle D Squires. Generation of turbulent inflow data for spatially-developing boundary layer simulations. *Journal of Computational Physics*, 140(2):233–258, 1998.

[25] Peter Bradshaw, DH Ferriss, and NP Atwell. Calculation of boundary-layer development using the turbulent energy equation. *Journal of Fluid Mechanics*, 28(3):593–616, 1967.

[26] Daniel Kempf, Min Gao, Andrea Beck, Marcel Blind, Patrick Kopper, Thomas Kuhn, , Marius Kurz, Anna Schwarz, and Claus-Dieter Munz. Development of turbulent inflow methods for the high order HPC framework FLEXI. In *High Performance Computing in Science and Engineering'21*. Springer. to appear.